PERGAMON

International Journal of Heat and Mass Transfer 42 (1999) 1925–1934

International Journal of HEAT and MASS TRANSFER

Detailed measurements of local heat transfer coefficients in turbulent flow through smooth and rib-roughened serpentine passages with a 180° sharp bend

S. Mochizuki[a,*], A. Murata[a], R. Shibata[a], Wen-Jei Yang[b]

[a] *Department of Mechanical Systems Engineering, Tokyo University of A&T, Koganei, Tokyo, 184-8588, Japan*
[b] *Department of Mechanical Engineering and Applied Mechanics, University of Michigan, Ann Arbor, MI, 48109, U.S.A.*

Received 20 November 1997; in final form 3 September 1998

Abstract

An experimental study is performed to investigate heat transfer and fluid flow in two straight, rectangular channels with a 180° sharp bend. Ribs are attached to two opposite walls with an angle of 90° or 60° to the flow. More than 450 thermocouples are used to monitor detailed distributions of local heat transfer coefficients over the four wall surfaces of the entire flow channel. Flow visualization tests are performed which reveal the generation of secondary flows. The impacts of their interaction on heat transfer enhancement and the rib arrangement which gives the highest heat transfer performance are disclosed. Applications to the internal cooling of gas turbine blades are discussed.

Key words: Local heat transfer coefficient; Heat transfer enhancement; Turbulent flow; Rib-roughened channel; 180° bend

Nomenclature

a width of the channel cross section [15 mm]
A total heat transfer surface area [wL]
A_c cross sectional area of the channel [ab]
b height of the channel cross section [30 mm]
c_p specific heat of air under constant pressure
d_e equivalent diameter [$4A_c/w$]
k thermal conductivity of air
L total length of the channel
$\dot{m}$ air mass flow rate
Nu local Nusselt number [$\alpha d_e/k$]
$Nu_{m,s}$ averaged Nusselt number for each of the four side walls
Nu_∞ Nusselt number for fluid-dynamically and thermally fully developed turbulent flow
Pr Prandtl number of air
$\dot{q}$ wall heat flux, eqn (1)
Re Reynolds number [$u_m d_e/v$]
T_b local bulk mean temperature of air, eqn (2)
$T_{b,1}$ test section inlet air temperature
$T_{b,2}$ test section outlet bulk mean air temperature
T_w local wall temperature
u_m mean air velocity in the channel [$\dot{V}/A_c$]
$\dot{V}$ volumetric flow rate of air
w perimeter of the flow cross section [$2(a+b)$]
z distance measured along the channel axis.

Greek symbols
α local heat transfer coefficient, eqn (3)
ϕ rib angle
v kinematic viscosity of air
ρ density of air.

1. Introduction

Numerous studies (e.g., [1–7]), have been performed to investigate flow and heat transfer characteristics in curved tubes in the absence of flow separation when the radius of curvature is relatively larger than the tube diameter. However, when a straight flow passage undertakes 180° bend, the combination of a secondary flow

* Corresponding author. Tel.: +81 (0)423 88 7088; fax: +81 (0)423 88 7088; e-mail: motizuki@cc.tuat.ac.jp

0017–9310/99/$ - see front matter
PII: S0017–9310(98)00308–1

induced by the centrifugal force and a large-scale flow separation causes extremely complex flow and heat transfer phenomena at both the bend region and the subsequent straight-flow section. Neither mechanisms nor characteristics of flow and heat transfer in such passages have been fully explored.

Flow passages with 180° sharp bends are common in the internal cooling passages within the blades of high-performance gas turbines. Flows in the flow passages of turbine blades are turbulent, with Reynolds numbers ranging from about 10^4–10^5, based on the hydraulic diameter of the flow passages as the characteristic lengths. In addition, ribs are installed on the walls of the straight passage region to promote heat transfer performance. Since the second half of the 1980s, enlarged-model flow passages have been employed in several experimental studies on heat transfer characteristics inside rib-roughened inward/outward flow passages with 180° sharp bends. These studies have sought to meet the need for enhanced turbine-blade cooling technology. They included: determination of the spatial distribution of mean heat transfer coefficients averaged over each passage increment [8–10], measurement of local mass transfer coefficients by means of the naphthalene sublimation method [11–16], measurement of local heat transfer coefficients along the flow passage using thermocouples [17, 18], and others. Flow and heat transfer in the flow passages downstream from sharp bends exhibit a highly three-dimensional nature. However, a few studies [19, 20] took that into account or conducted detailed measurements of the distribution of local heat transfer coefficient distributions on all four channel walls. On the other hand, some numerical simulation studies [21–23] were performed to predict heat transfer coefficient distributions. These results need to be verified by reliable test data.

With this background, the present study is focused on a model flow passage consisting of two straight rectangular ducts, with an aspect ratio of 2, which are connected by a 180° sharp bend. Both smooth and ribbed channel walls are tested. These channel wall temperatures are monitored using 458 thermocouples to investigate three-dimensional heat transfer characteristics. These include not only the axial- but also circumferential-distributions of heat transfer coefficients.

2. Experimental apparatus and procedure

The physical system studied is schematically illustrated in Fig. 1. It consisted of two straight ducts connected by a bend. The flow passage in each section was rectangular in cross section, 30 mm height × 15 mm width, with the equivalent diameter d_e of 20 mm. The flow lengths along the central axis were 210, 55 and 190 mm in the first pass, bend, and second pass, respectively. The sidewalls of the test section were made of Bakelite plates of 5 mm

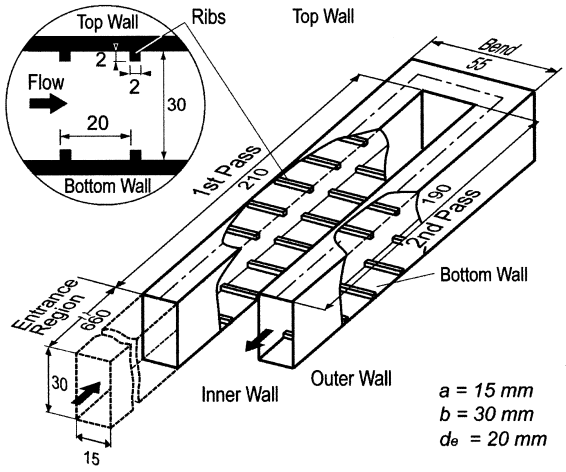

Fig. 1. Construction of test section.

thickness. An electric-conductive plastic film heater of 200 μm thickness (20 μm-thick electric conducting part, plus 180 μm-thick base) was placed over the entire inner wall surface. A polyurethane foam insulating material, approximately 10 mm thick, covered the entire test section. In the present study, in addition to the smooth flow passage case, tests were also performed on flow passages fitted with symmetrical ribs of various patterns. These were installed on both the top and bottom walls in the first and second passages. These ribs were made of Bakelite with 2 × 2 mm cross sections at a longitudinal pitch (along the flow axis) of 20 mm irrespective of rib patterns. Figure 1 illustrates ribs installed at a 90° angle. After flow-rate measurements were taken by means of laminar-flow type flowmeter, the air from a turbo-blower passed through a honeycomb-type flow rectifier into the test section via a 660 mm long entrance region.

The local heat-transfer surface temperature inside the test section was monitored by means of 50 μm diameter K-type thermocouples installed underneath the film heater. Figure 2 shows the locations of 458 thermocouples; 127 each on the top and bottom walls, 93

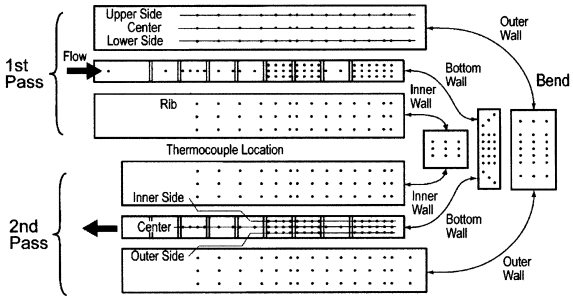

Fig. 2. Thermocouple locations.

on the inner wall and 111 on the outer wall. A K-type thermocouple was positioned at the inlet to the entrance region to measure the test-section inlet temperature, $T_{b,1}$. A well-insulated mixing chamber consisting of four hole-type baffles was set up at the exit from the test section. A copper wire grid onto which multiple thermocouples were soldered was installed across the duct cross section immediately behind the mixing chamber. These thermocouples were joined in series to form a thermocouple pile to measure the exit mixed-mean temperature, $T_{b,2}$. The heat flux from the duct walls, $\dot{q}$, was evaluated using the expression:

$$\dot{q} = \dot{m}c_p(T_{b,2} - T_{b,1})/A \quad (1)$$

Here, $\dot{m}$ denotes the mass flow rate of air; c_p, specific heat under constant pressure; A, total heat transfer area [wL]; w, perimeter of the flow cross section and L, total length of the test section. The local mixed-mean fluid temperature, T_b, at the axial distance, z, is considered to linearly increase with z. This approximation is justified under the uniform heat flux condition which prevails in the present case with electrical heating. T_b can thus be determined as

$$T_b = T_{b,1} + (z/L)(T_{b,2} - T_{b,1}) \quad (2)$$

The local heat transfer coefficient, α is equal to

$$\alpha = \dot{q}/(T_w - T_b) \quad (3)$$

Figure 3 depicts the symbols representing the location of thermocouples around the circumferential direction of the flow cross section. They are used in the succeeding figures to indicate the corresponding locations, unless defined otherwise. In addition to smooth flow passages, the present study includes testing of ribbed surfaces with rib angles, $\phi = 90$ and 60°. Tests on the 60° ribbed surfaces include four distinct patterns of rib arrangement as shown in Fig. 4: PP, PN, NP and NN. In each case, the rib patterns are parallel on both the top and bottom walls. Taking into consideration secondary flow (i.e., pairs of vortices) induced by inclined ribs, two different situations may arise. One is when the direction of the secondary flow induced by inclined ribs coincides with that of the secondary flow induced by the bend. This will be referred to as positive, or 'P'. The other situation is if the directions of these two secondary flows are opposite which will be called negative, or 'N'. Henceforth, P and N will be used to describe the rib pattern in the straight flow passes. For example, PN means that the rib arrangement in the first pass is P while that in the second pass is N.

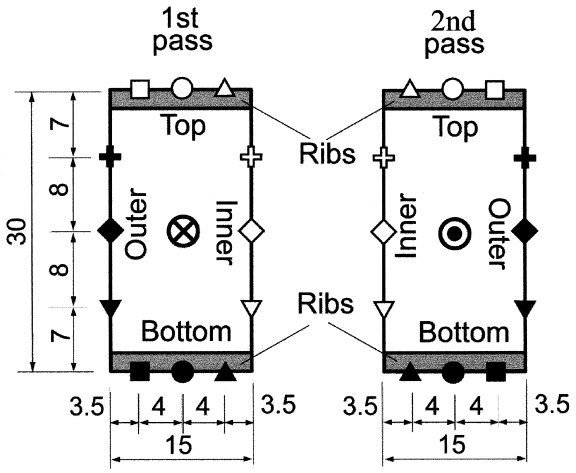

Fig. 3. Symbols indicating circumferential locations of thermocouples.

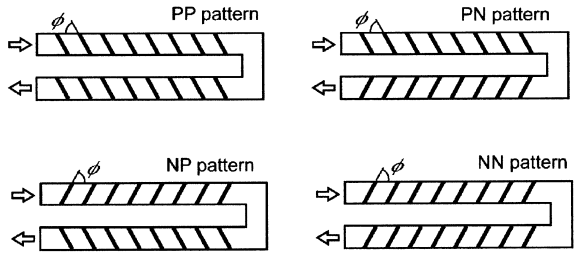

Fig. 4. Combination of rib patterns.

3. Experimental results and discussion

In the interest of brevity, only results for the $Re = 15\,000$ case are presented here to investigate the effects of rib arrangement patterns on the distribution of the local Nusselt number, Nu. Notice that both the Reynolds and Nusselt numbers are defined based on the equivalent diameter, d_e, as the characteristic length, with the mean flow velocity, u_m, in the flow cross section as the characteristic velocity.

3.1. Smooth top and bottom walls

Results for the smooth flow passage are illustrated in Fig. 5. The axial distributions of the Nusselt number normalized by that for a fully-developed turbulent flow in a straight tube, Nu/Nu_∞, are presented in Fig. 5(a), (b), (c) and (d) for the top, bottom, inner and outer walls, respectively. The abscissa, z/d_e, is the distance from the inlet of the test section along the central axis of the flow passage being normalized by the hydraulic diameter. The borderline between the first pass and the bend, and that between the bend and the second pass, are $z/d_e = 10.5$ and 13.25, respectively. Here, the empirical equation for Nu_∞ in Kays and Crawford [24], $Nu_\infty = 0.022Re^{0.8}Pr^{0.5}$, is employed where Pr is the Prandtl number. The curve in each figure represents the Nusselt number distribution

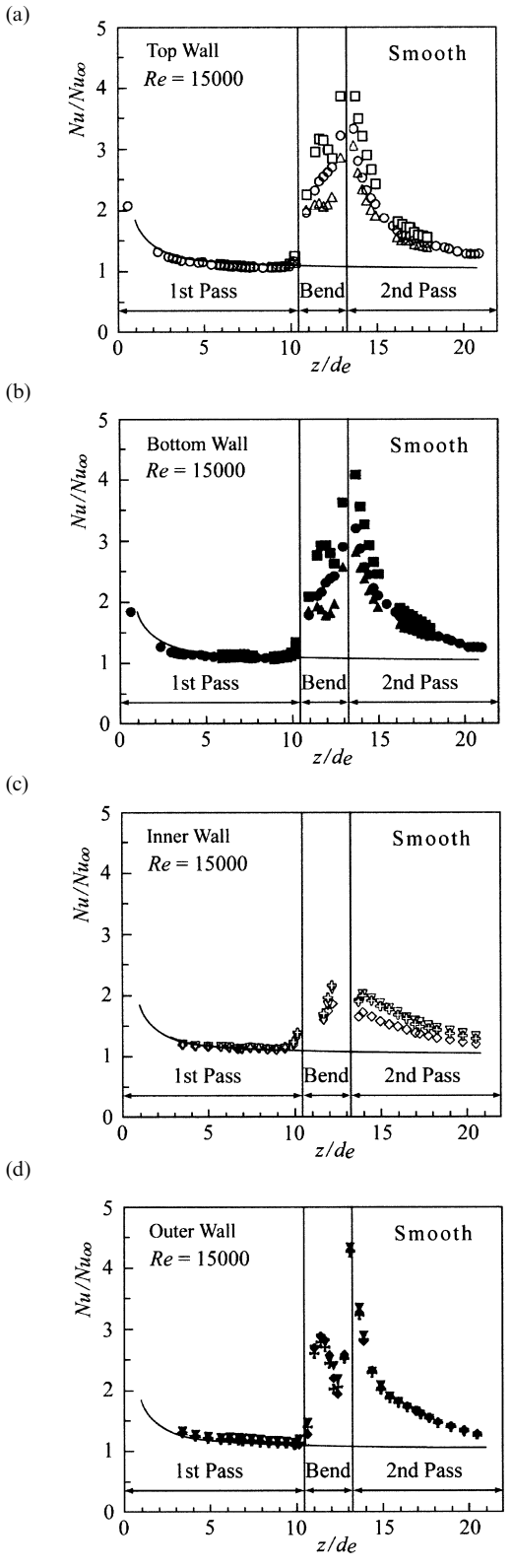

Fig. 5. Axial distribution of Nu/Nu_∞ on each wall of smooth channel.

in the entrance region of a turbulent flow in a straight tube [25]. It is apparent from the figures that:

(1) The *Nu* distributions on all four walls in the first pass correlate well with the traditional empirical equation, thus verifying the reliability of the present test setup.
(2) The *Nu* values on all four walls begin to rise immediately before the inlet to the bend and continue to increase after entering the bend. Their subsequent behavior within the bend differs with each individual wall as follows:

    The *Nu* behaviors of the top and bottom wall within the bend are practically identical due to the symmetry of thermal-fluid phenomena. However, their magnitudes on the outer-wall side are always higher than those of the centerline, while their values on the inner-wall side are always lower than those of the centerline. Note especially that the *Nu* values on the outer-wall side are about the same magnitude as the *Nu* values on the outer wall, to be described later.

(3) Although the increase in *Nu* on the inner wall in the bend is the lowest of the four walls, its highest value is over twice that of the straight tube cases.
(4) Of the four walls in the bend, *Nu* is highest on the outer wall. The *Nu* values on the outer wall are practically uniform in the lateral direction. They undergo a steep increase with z/d_e in the bend, then fall, then very steeply increase to achieve a maximum value near the exit. In other words, there are two locations in the bend where the *Nu* on the outer wall reaches maxima. The second maximum *Nu* is the highest of the entire flow passage, surpassing by four times the maximum *Nu* in a straight tube.
(5) It is at the inlet to the second pass where the *Nu* values on both the top and bottom walls reach maxima. These maxima are comparable to that on the outer wall, reaching almost four times that of a straight tube.
(6) In the second pass, *Nu* values on all four walls decrease monotonically with z/d_e and asymptotically approach the *Nu* in the straight tube case.

Figure 6 depicts the *Nu* distribution in the circumferential direction of the flow cross section near the entrance to the second pass (for $z/d_e = 13.6$ and 14.4). It is clear from the figure that (1) the maximum *Nu* is not on the outer wall which confront the turning flow, but rather occurs at the top and bottom walls; and (2) the *Nu* distributions in the lateral direction are relatively uniform on the outer and inner walls. By contrast, the *Nu* distributions on the top and bottom walls diminish significantly from the outer toward the inner walls.

Hence, in the case of two-way flow passages connected by a 180° sharp bend, *Nu* values on each wall downstream from the bend are significantly enhanced even in the

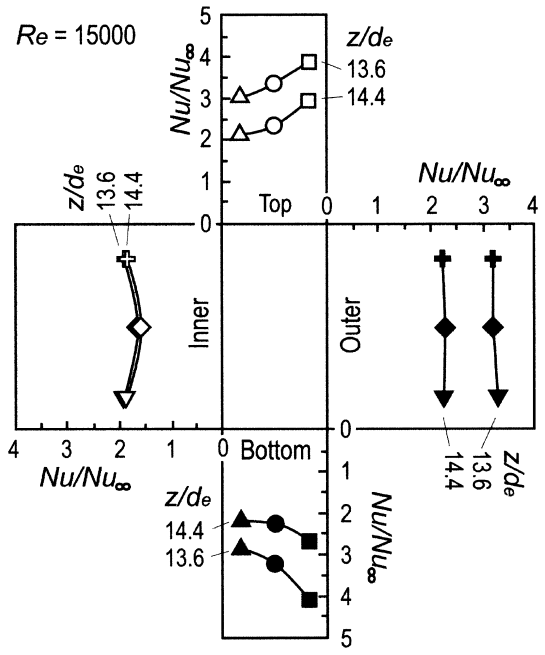

Fig. 6. Circumferential distribution of Nu/Nu_∞ in the inlet region of 2nd pass.

smooth-wall case. The *Nu* distributions exhibit characteristic of three-dimensional flow structures. To the authors' knowledge, this is the first work to reveal detailed convective three-dimensional heat transfer characteristics in and after the 180° sharp bend. In order to explore the mechanism of these heat transfer characteristics, a flow visualization study was performed on airflow, utilizing paraffin mist as the tracer and a laser light sheet as the light source. Representative photographs are presented in Fig. 7. In the figure, (a) corresponds to the flow on the midplane between the top and bottom walls, and (b) and (c) are the flows on the X–X and Y–Y planes, respectively. The flow cross section used in the flow visualization is square (44 × 44 mm) and the Reynolds number based on the hydraulic diameter is 500. A separation from the corner of the inner wall, vortices generated at each corner of the outer wall, secondary flow vortices observed in (b) and (c), and their rotating directions, are all considered to be qualitatively similar to those in the present heat transfer experiments. The following phenomena are revealed: the flow that enters the bend via the first pass impinges on the confronting surface (i.e., outer wall) of the bend at the location shown in the figure by the arrow **A**. A portion of that flow runs downstream in the axial direction along the outer wall, another part undergoes a reverse flow, and the remaining stream turns in the lateral direction of the outer wall, thus forming a secondary flow. The downstream flow along the outer wall detaches at the second corner but reattaches to the outer wall at the location illustrated by the arrow **B**. It is believed that the two maxima (Fig. 5(d)) in the *Nu* distribution in the axial direction of the outer wall in the bend correspond to these two reattachment points.

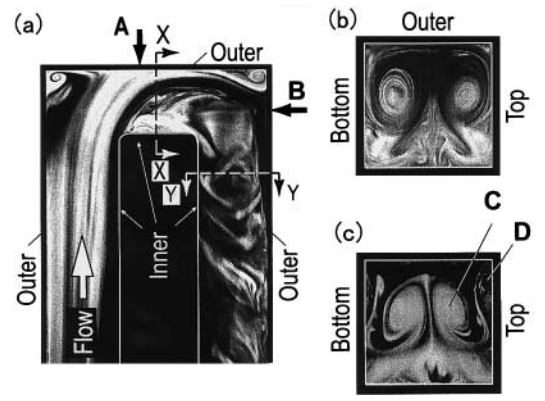

Fig. 7. Visualized flow behavior in the bend. (a) Mid plane between top and bottom wall; (b) section X–X; (c) section Y–Y.

Since the centrifugal force acts on the flow making a turn in the bend, the higher velocity flow is forced toward the outer wall. As a result, the secondary flows are induced as shown in Fig. 7(b) and (c). Figure 7(b) exhibits the secondary flow that is induced near the original reattachment point. It transports the fluid from the region away from the wall surface, with a greater momentum but a lower temperature, toward the outer wall surface. Subsequently, the fluid flows along the top and bottom walls from the outer toward inner walls. The heat transfer from the outer wall and the two sidewalls is consequently enhanced. It is seen in Fig. 7(c) that, in addition to the main vortex **C**, secondary vortices appear on both the top and bottom walls near the outer-wall side, as indicated by **D**. The phenomenon can be clearly observed in a video tape. These second vortices fail to appear in Fig. 7(b). The authors consider this to be the reason why the Nusselt numbers on the top and bottom walls (especially near the outer-wall side) at the inlet to the second pass are either the same as, or higher than, those on the outer wall.

3.2. Rib-roughened top and bottom walls

Figure 8 depicts the *Nu* distributions on the walls of rib-roughened channels, with (a), (b) and (c) being the rib patterns of 90°, 60° PP and 60° NN (referring to Fig. 4), respectively. Note that the *Nu* distributions on the bottom wall are practically identical to those on the top wall and so are omitted here. The following items are revealed in the figure:

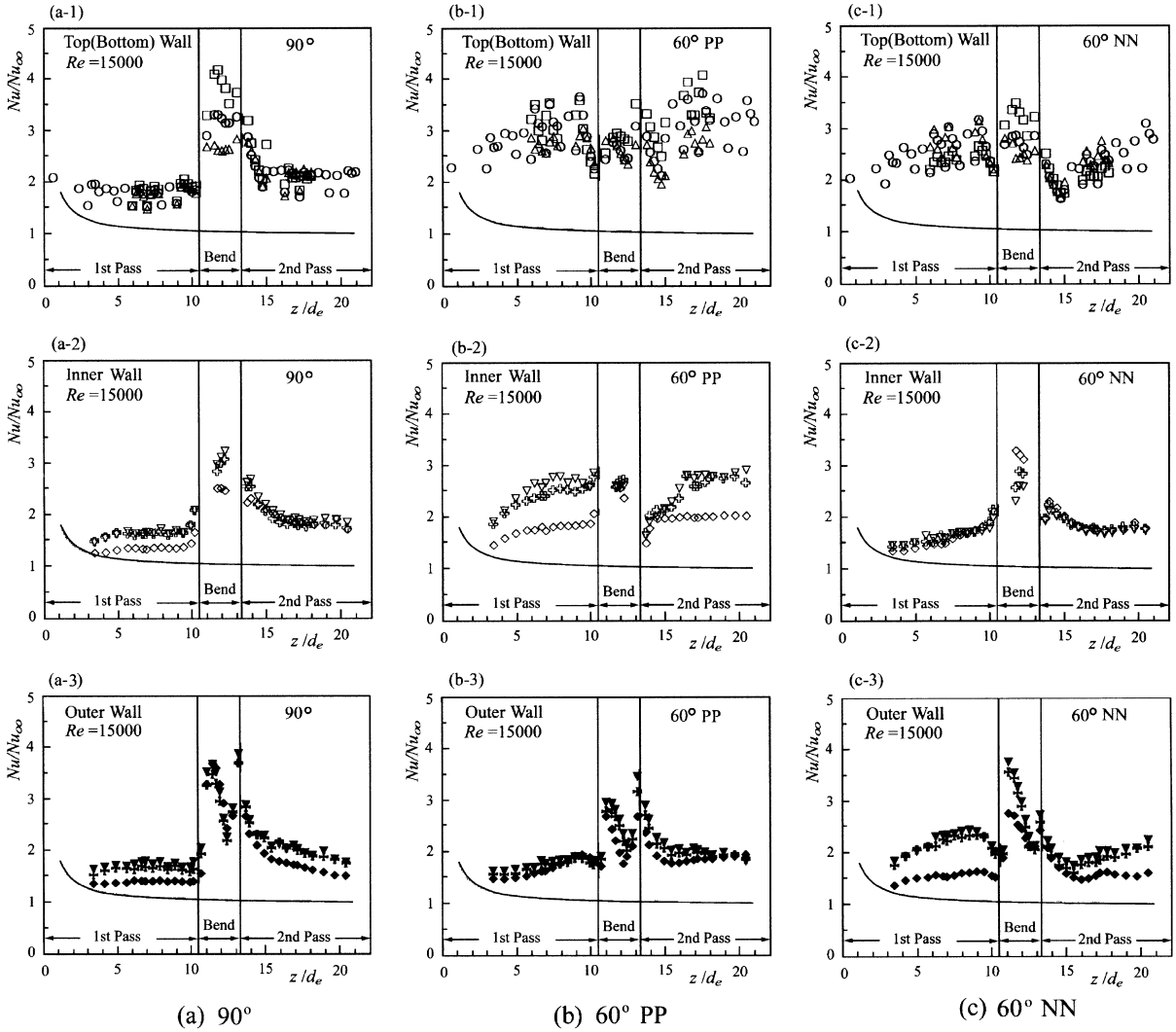

Fig. 8. Axial distribution of Nu/Nu_∞ on each wall of rib-roughened channels.

(1) In all three cases of the three rib-roughened channels (Fig. 8(a), (b) and (c)), *Nu* values on the four wall surfaces are significantly higher than those on the smooth channel wall (Fig. 5), except in the bend and its immediate neighborhood. This suggests that the ribs have a significant effect on heat transfer augmentation. It is especially noteworthy that the *Nu* values are also enhanced on both the inner and outer walls where no ribs are attached.

(2) In the straight flow passages (excluding their portions at the immediate inlet and exit of the bend) the *Nu* values in the flow channels attached with inclined ribs (b) and (c) follow a trend of gradual growth with an increase in z/d_e. In the case of 90° ribs in (a), the Nusselt number is maintained at a nearly constant value. This contrasts with the smooth channel case (Fig. 5) in which the *Nu* diminishes gradually, with an increase in z/d_e in the straight portion.

(3) In almost the entire first pass, and the second half of the second pass, the inclined ribs induce a higher heat transfer than do the 90° ribs, irrespective of whether the pattern is PP or NN.

(4) The inclined ribs taking either the PP or NN pattern can significantly affect the *Nu* distribution on the inner and outer walls in the straight flow passages (comparing (b-2) with (c-2) and (b-3) with (c-3)). In the first pass, however, there are symmetries in the *Nu* distributions between the cases (b-2) for the inner wall of the PP pattern, and (c-3) for the outer wall of the NN pattern. There are also symmetries between the cases (b-3) for the outer wall of the PP pattern and (c-2) for the inner wall of the NN pattern.

(5) This symmetry in the *Nu* distributions is no longer seen in the bend and second pass.
(6) When inclined ribs are attached, the *Nu* values on the top and bottom walls in the bend ((b-1) and (c-1)) are significantly lower than those of the smooth channels and 90° rib-roughened channels (a-1).

Heat transfer enhancement in the 90° rib-roughened wall is due to the combined effects of flow separation/reattachment and the flow mixing caused by flow instability. On the other hand, when ribs are placed at a certain angle to the flow, a new flow is induced along the ribs other than the separated flow from the ribs. Figure 9 presents measured *Nu* distributions along the top walls with 90° ribs (left figure) and 60° PP inclined ribs (right figure) in the midportion of the first pass. One can see that the *Nu* for the 90° ribs is practically uniform in the lateral direction but varies periodically in the axial direction in tandem with the rib pitch. This is because the *Nu* diminishes in the separated flow region immediately behind the ribs, achieves the maximum value near the reattachment point, and then decreases with the development of a boundary layer until the next rib, thus forming a cycle that is repeated from rib to rib. In the case of inclined 60° PP ribs shown in the right figure of Fig. 9, *Nu* not only periodically varies in the flow direction but also diminishes along the ribs from the outer wall toward the inner wall. The combination of flow separation/reattachment due to the presence of ribs and a flow along the inclined ribs causes a significant augmentation in the heat transfer performance (see preceding item (3)). The flow induced along the ribs on the top and bottom walls enhances the *Nu* on the wall confronting the flow (for example, the inner wall in case of the PP pattern and the outer wall in case of the NN pattern) (item (4)). Those flows induce secondary flows inside the channels which are symmetrical with respect to a midplane between the top and bottom walls. Inside the rib-roughened channels, these secondary flows grow stronger each time they cross over the ribs in their downstream direction. This results in an augmentation of *Nu* with z/d_e (item (2)). Although the rotating direction of the secondary flow induced by the ribs depends upon the rib patterns, that of the secondary flow formed at the bend remains unchanged (refer to Fig. 7). The heat transfer characteristics in the first pass are symmetrical (item (4)) because the flows at P and N are symmetrical. However, the flow/heat transfer characteristics are affected by the rib patterns of the first pass, in the case of the bend, and by that of both the first and second passes in the case of the second pass (item (5)). The reason for the large reduction in heat transfer (item (6)) is still unclear and requires further investigation of the three-dimensional flow phenomena in the bend.

Figure 10 illustrates the circumferential distribution of *Nu* at the midpoint ($z/d_e = 16.4$) in the second pass. Nu/Nu_∞ for the PP and NN rib patterns is compared. The figure reveals that the *Nu* distributions for the PP and NN rib patterns in the second pass are qualitatively symmetrical. In other words, the top and bottom wall temperatures diminish from the outer toward the inner walls in the PP case but increase in the NN case. Furthermore, the temperature distribution shapes of the PP and NN rib patterns are reversed on the inner and outer walls. The qualitative trend of heat transfer characteristics unique to each rib pattern in the first pass, is also seen in the second pass. However, quantitatively, on all

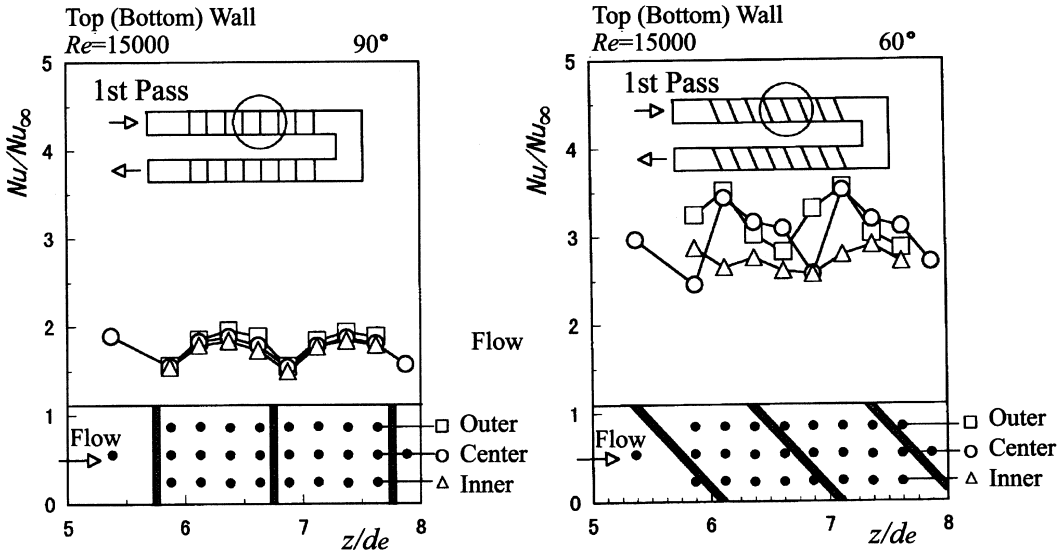

Fig. 9. Comparison of Nu/Nu_∞ distributions between 90° (left) and 60° (right) ribs, top (bottom) walls, 1st pass.

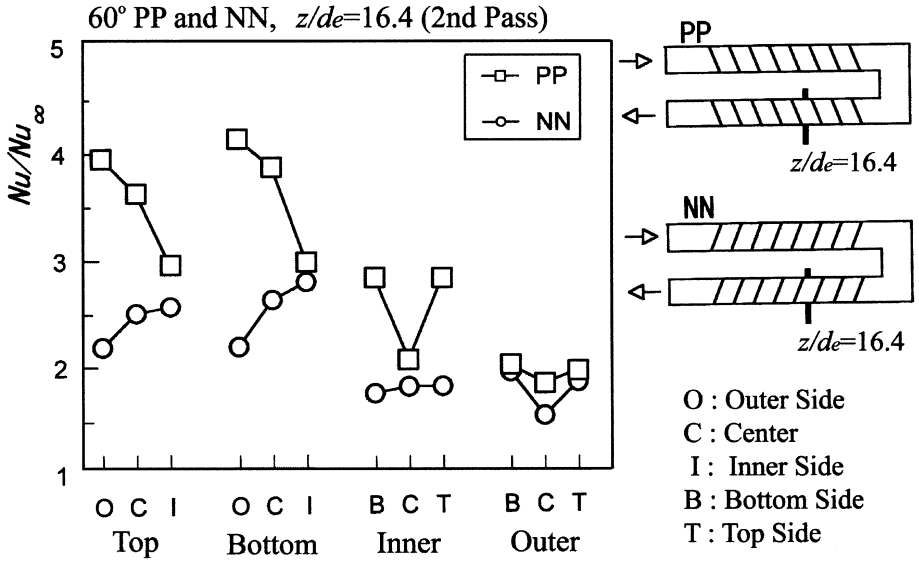

Fig. 10. Comparison of circumferential distribution of Nu/Nu_{∞} between PP and NN, 60° rib, $z/d_e = 16.4$.

four wall surfaces the PP rib patterns exhibit a higher Nu distribution than the NN rib patterns. One thing is clear from the Nu distributions on all wall surfaces in the second pass (with the 60° PP and 60° NN rib patterns in Fig. 8(b) and (c) respectively); the trend is found not only in the present example (selected at the location $z/d_e = 16.4$), but throughout nearly the entire pass. This phenomenon can be attributed to an interaction between a flow formed through the first pass and the bend, and another flow induced by the rib patterns in the second pass.

Figure 11 illustrates how different rib patterns (PP, PN, NP and NN) at 60° angles can affect the average Nusselt number, $Nu_{m,s}$ on each of the four wall surfaces, (top, bottom, inner and outer) in the second pass. Results for 90° rib-roughened and smooth channels are superimposed on the figure for comparison. It can be seen in the figure that (1) on all four wall surfaces, irrespective of rib patterns, the 60° inclined ribs have higher average Nusselt numbers than the 90° ribs, and both have higher $Nu_{m,s}$ than the smooth channels. (2) The top and bottom walls with 60° PP rib patterns exhibit the best heat transfer performance. In an application of ribs to the internal cooling of gas turbine blades, the rib-roughened wall surfaces (corresponding to the top and bottom surfaces in the present study) should have high convective heat transfer coefficients and be spatially uniform. For example, it is undesirable to have a steep heat transfer coefficient in the bend of the channel. Judging from the data presented so far, one must conclude that surfaces with 60° PP rib patterns are the most suitable for this purpose.

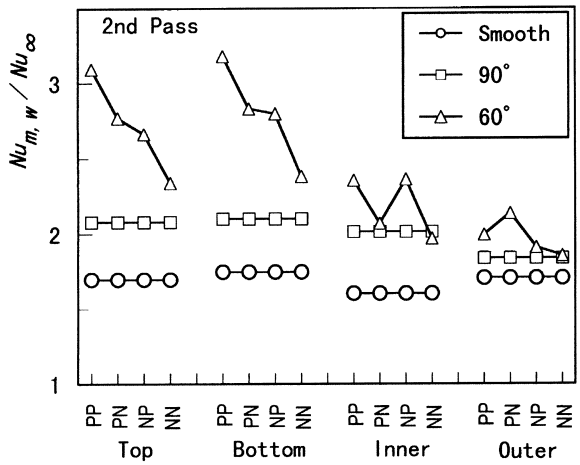

Fig. 11. Effect of rib arrangements on mean Nusselt number of each of the four surfaces, 2nd pass.

The channel cross section being studied here is rectangular, with an aspect ratio of 2, and with ribs attached on the shorter side. Since the distance between the two shorter sides is longer than that between the two longer sides, the effects of the ribs on flow are less than in the case of a channel with a smaller aspect ratio (such as a square channel). That is, those special features induced by the ribs that are revealed in the present experiment are thought to be more pronounced in smaller aspect-ratio channels.

4. Conclusions

Detailed measurements of local heat transfer coefficients have been taken from two straight channels of an aspect ratio of 2 connected by a 180° sharp bend. The two opposite wall surfaces of the channel were either roughened with ribs (of 90 and 60° inclined) or smooth. The following conclusions were reached:

4.1. The smooth flow passage case

(1) Heat transfer characteristics downstream from the bend are controlled by secondary flows generated in the bend. The heat transfer coefficient distribution on each wall surface differs substantially from others.
(2) The highest heat transfer coefficient throughout the entire flow passage appears on the outer wall near the exit from the bend (in the neighborhood of the second boundary-layer reattachment point). Its magnitude exceeds by four times that of straight tube case.
(3) Regions with high heat transfer coefficients of approximately the same value as in item (2) exist on both the top and bottom walls, near the outer wall of the inlet to the second passage. This is believed to be due to the formation of a second flow vortex.

4.2. The rib-roughened duct case

(1) The presence of 90° ribs causes an enhancement in the heat transfer coefficient over the smooth flow passage case practically throughout the entire duct. On the other hand, inclined ribs induce secondary flows due to the occurrence of flow along the ribs as well as flow separation/reattachment. As a result, heat transfer coefficients higher than the 90°-rib case prevail except in the bend and in its immediate downstream region.
(2) In the inclined-rib-roughened flow passage, an interaction occurs between two secondary flows, one induced by the ribs and the other by the bend. Due to this interaction, the rib patterns in the first pass and both two passes strongly influence heat transfer characteristics in the bend and second pass, respectively. For example, the PP rib pattern gives higher average heat transfer coefficients on all four wall surfaces in the second pass than does the NN rib pattern (see Fig. 4).
(3) The heat transfer performance on the rib-roughened surfaces in the second pass achieves maximum value with the installation of 60° inclined ribs arranged in the PP pattern.

References

[1] K.C. Cheng, M. Akiyama, Laminar forced convection heat transfer in curved rectangular channels, International Journal of Heat and Mass Transfer 13 (1970) 471–490.
[2] D.E. Metzger, C.W. Plevich, C.S. Fan, Pressure loss through sharp 180 deg turns in smooth rectangular channels, Trans. ASME, Journal of Engineering for Gas Turbines and Power 106 (1984) 677–681.
[3] J.A.C. Humphrey, H. Iacovides, B.E. Launder, Some numerical experiments on developing laminar flow in circular-sectioned bends, J. Fluid Mech. 154 (1985) 357–375.
[4] T. Kajishima, Y. Miyake, T. Inaba, Numerical simulation of laminar flow in curved ducts of a rectangular cross-section, Trans. JSME, B 54:(503) (1985) 1594–1601.
[5] S. Sugiyama, M. Yamamoto, T. Hayashi, Flows in a curved rectangular channel (2nd report, velocity measurements in the developing region of laminar flow by using LDV), Trans. JSME,. B 53(487) (1987) 750–756.
[6] K.C. Cheng, F.P. Yuen, Flow visualization studies on secondary flow patterns in straight tubes downstream of a 180-degree bend and in isothermally heated horizontal tubes, Trans. ASME, Journal of Heat Transfer 109 (1987) 49–54.
[7] G.J. Hwang, C.H. Chao, Forced laminar convection in a curved isothermal square duct, Trans. ASME Journal of Heat Transfer 113 (1991) 48–55.
[8] D.E. Metzger, C.S. Fan, C.W. Plevich, Effects of transverse rib roughness on heat transfer and pressure losses in rectangular ducts with sharp 180 degree turns, AIAA Paper No. 88-0166 (1988) 1–8.
[9] J.H. Wagner, B.V. Johnson, R.A. Graziani, F.C. Yeh, Heat transfer in rotating serpentine passages with trips normal to the flow, Trans. ASME, Journal of Turbomachinery 114 (1992) 847–857.
[10] B.V. Johnson, J.H. Wagner, G.D. Steuber, F.C. Yeh, Heat transfer in rotating serpentine passages with trips skewed to the flow, ASME Paper 92-GT-191 (1992).
[11] P.R. Chandra, J.C. Han, S.C. Lau, Effect of rib angle on local heat/mass transfer distribution in a two-pass rib-roughened channel, ASME Journal of Turbomachinery 110 (1988) 233–241.
[12] J.C. Han, P.R. Chandra, S.C. Lau, Local heat/mass transfer distributions around sharp 180-deg turns in two-pass smooth and rib-roughened channels, Trans. ASME, Journal of Heat Transfer 110 (1988) 91–98.
[13] M.K. Chyu, Regional heat transfer in two-pass and three-pass passages with 180-deg sharp turn, Trans. ASME, Journal of Heat Transfer 113 (1991) 63–70.
[14] M. Hirota, H. Fujita, A. Tanaka, M. Taki, Characteristics of local heat (mass) transfer in rectangular ducts with a sharp 180-degree turn, 32nd National Heat Transfer Symposium of Japan 1 (1995) 39–40.
[15] M. Hirota, H. Fujita, T. Yoshida, S. Araki, T. Tanaka, Characteristics of local heat (mass) transfer in rectangular ducts with a sharp 180-degree turn (influences of flow inlet condition), 33rd National Heat Transfer Symposium of Japan 3 (1996) 605–606.
[16] M.K. Chyu, Regional heat transfer and pressure drop in two-pass and three-pass flow passages with 180-degree sharp turns, ASME Paper 89-GT-191 (1989) 1–8.
[17] W.-J. Yang, N. Zhang, J. Chiou, Local heat transfer in a rotating serpentine flow passage, Trans. ASME, J. of Heat Transfer 114 (1992) 354–361.
[18] S. Mochizuki, J. Takamura, S. Yamawaki, W.-J. Yang, Heat transfer in serpentine flow passage with rotation, Trans. ASME, J. of Turbomachinery 116 (1994) 133–140.

[19] A. Murata, S. Mochizuki, M. Fukunaga, Detailed measurement of local heat transfer in a square-cross-section duct with a sharp 180-degree turn, in: Proceedings of the Tenth International Heat Transfer Conference, Brighton, U.K., 8-IC-19 (1994) 291–296.
[20] S. Mochizuki, A. Murata, M. Fukunaga, Effect of rib arrangements on pressure drop and heat transfer in a rib-roughened channel with a sharp 180-degree turn, Trans. ASME, J. of Turbomachinery 119 (1997) 610–616.
[21] R.W. Johnson, Numerical simulation of local Nusselt number for turbulent flow in a square duct with a 180° bend, Numerical Heat Transfer 13 (1988) 205–228.
[22] D.L. Besserman, S. Tanrikut, Comparison of heat transfer measurements with computations for turbulent flow around a 180-degree bend, Trans. ASME, Journal of Turbomachinery 114 (1992) 865–871.
[23] T.S. Wang, M.K. Chyu, Heat convection in a 180-degree turning duct with different turn configurations, Journal of Thermophysics and Heat Transfer 8(3) (1994) 595–601.
[24] W.M. Kays, M.E. Crawford, Convective Heat and Mass Transfer, 2nd ed., McGraw-Hill, 1980, p. 243.
[25] JSME, Heat Transfer Data Book, JSME, 4th ed., 1986, p. 57.